Epitaxial checkerboard arrangement of nanorods in $ZnMnGaO_4$ films studied by x-ray diffraction

S. M. O'Malley,* P. L. Bonanno, K. H. Ahn, and A. A. Sirenko
Department of Physics, New Jersey Institute of Technology, Newark, New Jersey 07102, USA

A. Kazimirov
Cornell High Energy Synchrotron Source (CHESS), Cornell University, Ithaca, New York 14853, USA

M. Tanimura
Department of Research, NISSAN ARC, LTD., Yokosuka, Kanagawa 237-0061, Japan

T. Asada
Department of Research, NISSAN ARC, LTD., Yokosuka, Kanagawa 237-0061, Japan
and Rutgers Center for Emergent Materials and Department of Physics and Astronomy, Rutgers University, Piscataway, New Jersey 08854, USA

S. Park, Y. Horibe, and S-W. Cheong
Rutgers Center for Emergent Materials and Department of Physics and Astronomy, Rutgers University, Piscataway, New Jersey 08854, USA

(Received 15 April 2008; revised manuscript received 19 August 2008; published 27 October 2008)

The intriguing structural properties of a $ZnMnGaO_4$ film epitaxially grown on MgO (001) substrate have been investigated using synchrotron-radiation-based x-ray diffraction. The $ZnMnGaO_4$ film consisted of a self-assembled checkerboard (CB) structure with highly aligned and regularly spaced vertical nanorods. The lattice parameters of the orthorhombic and rotated tetragonal phases of the CB structure were analyzed by measuring *H-K*, *H-L*, and *K-L* cross-sectional reciprocal space maps. We demonstrate that symmetry of lattice distortions at the phase boundaries provides means for the coherent coexistence of two domain types within the film volume.

DOI: 10.1103/PhysRevB.78.165424 PACS number(s): 81.16.Dn, 61.46.−w, 61.05.cp

I. INTRODUCTION

The precise control of domains and phase separation on the nanoscale can provide new technological advantages for monolithic integration of materials with complementary electronic and magnetic properties. Recent interest in growth techniques which are not restricted by spatial resolution, e.g., lithography, but rather based on self-organization has resulted in the discovery of several material systems with periodic nanocheckerboard (CB) patterns.[1–7] Synthesis of spinel oxides with CB structures, such as nonmagnetic $ZnMnGaO_4$ (ZMGO) (Ref. 1) and magnetic Mn-doped $CoFe_2O_4$,[4] relies on harnessing Jahn-Teller (JT) distortions in the solid phase during growth to form nanoscale domain structures. For example, the self-assembled CB structure in bulk polycrystalline ZMGO (Ref. 1) occurs during the annealing process: Upon cooling the high-temperature cubic ZMGO phase experiences JT distortion into a lower-symmetry tetragonal phase, inducing a miscibility gap within the system of mixed JT ions and subsequently spinoidal decomposition. The mixture then experiences a diffusion-type spatial separation into Mn-rich and Mn-poor regions. The alternating Mn-rich (tetragonal) and Mn-poor (cubic) regions can then coexist by producing a strain-accommodating CB structure.[1,3,4,8,9] An important step toward utilization of this intriguing phenomenon for large-scale planar device technology as recently reported in Ref. 5 is the epitaxial growth of thin CB films. In this paper we discuss structural properties of these $ZnMnGaO_4$ films, such as lattice parameters, strain relaxation effects, and lattice distortions at the domain boundaries.

II. EXPERIMENTAL METHODS

The ZMGO film was grown by pulsed laser deposition (PLD) on a single-crystal MgO (001) substrate ($a=0.4212$ nm) using a KrF excimer laser. The target material was the homogenous high-temperature-quenched form of ZMGO with a tetragonal lattice ($a=0.82$ nm and $c=0.87$ nm). The CB patterned epilayer is formed of two periodically alternating and structurally different spinel phases: (i) rotated tetragonal (Mn-poor and JT inactive) and (ii) orthorhombic (Mn-rich and JT-active) phases. These regularly spaced nanodomains have a typical size of $4\times4\times750$ nm^3 and are highly aligned along the growth direction. A significant number of ZMGO films have been grown, which show consistency in the formation of a checkerboard structure.[5]

X-ray diffraction measurements were carried out at the A2 beamline of Cornell high-energy synchrotron source (CHESS), where the high brilliance and large photon flux characteristic of synchrotron radiation were beneficial in shortening the otherwise lengthy measurement of reciprocal space maps (RSMs) and in detecting weak diffraction signals

from the CB structure. The incident synchrotron beam was conditioned using a double-bounce Si (111) monochromator passing photons with an energy of 10.53 keV. High angular resolution was achieved by conditioning the diffracted beam using a single-bounce Si (111) analyzer crystal. RSMs of the CB structures were analyzed for several symmetric and asymmetric reflections: (002), (−202), (−2−22), (004), and (044). In the following, Miller index L corresponds to the film-growth direction, while H and K represent the in-plane parameters of the structure. The integer values of H, K, and L correspond to the reciprocal-lattice points (RLPs) of a reference spinel structure with lattice parameter a_S=0.8424 nm (twice the value of that for the cubic MgO substrate). In this notation a strong (022) diffraction peak of MgO substrate coincides with the (044) RLP of the reference spinel structure.

III. RESULTS

Performing a series of symmetric and asymmetric cross-sectional RSMs has allowed for the determination of both in-plane and out-plane lattice parameters along with structural distortion properties within the CB structure. The *H-K*, *H-L*, and *K-L* cross sections around the (044) and (004) RLPs are compared in Figs. 1(a) and 1(b). The *H-K* map for the (044) reflection [Fig. 1(a)] is dominated by several peaks associated with different phases within the CB film. In Ref. 5 we attributed the four broad peaks labeled α, β, γ, and δ to two conversely rotated tetragonal (β and γ) and two perpendicularly oriented orthorhombic (α and δ) phases. The four diagonal peaks (ρ, σ, τ, and υ) in Fig. 1(a) have been associated with distortions originating from domain boundaries and will be discussed in detail later. The α, β, γ, and δ peak centers occur at the same out-plane value L=4.07 [see side panels in Fig. 1(a)]. This observation indicated that all CB associated phases have the same out-plane lattice parameter (c_{CB}=0.829 nm), which is crucial for their coexistence within the film volume. (It should be noted that this value is close to that of the bulk polycrystalline phase of ZMGO).[1] The MgO substrate peaks lay outside the mapped areas at the integer reciprocal-lattice points. The average in-plane lattice parameters of the two rotated tetragonal phases are practically lattice matched to the substrate, i.e., the tetragonal phase is elastically strained with a_{tet}=0.841 nm. The centers of these peaks (β and γ) are rotated by ±2.55° around the (00L) reciprocal-lattice vector. The assignment of the rotation axis is based on comparison with RSMs measured at the symmetric (004) reflection. In contrast to the (044) reflection, the *H-K* cross section for the (004) reflection [Fig. 1(b)] illustrates all of the CB peaks have collapsed into a single peak around H=K=0. The corresponding intensity maximum maintains the same value of L=4.07 as that for the (044) reflection [see side panels in Fig. 1(b)]. The presence of any discreet tilting of the CB arranged nanorods has been ruled out by the observation in Fig. 1(b) of only a single central peak.[10] The orthorhombic phases α and δ have short and long in-plane lattice parameters a_{otho}=0.814 nm and b_{otho}=0.898 nm, respectively, and are therefore inelastically strained. A summary of the structural parameters of the CB

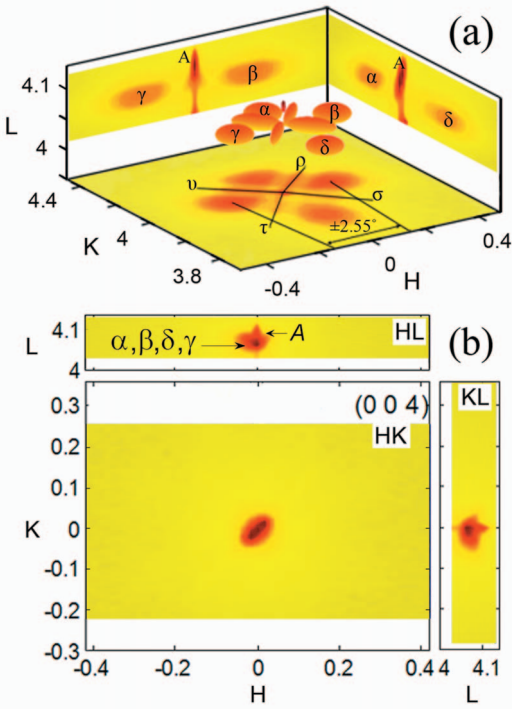

FIG. 1. (Color). (a) The *H-K*, *H-L*, and *K-L* cross-sectional RSM measured around the asymmetric (044) reflection with L =4.08. The α and δ peaks are orthorhombic phases, while the β and γ peaks are rotated tetragonal phases associated with the CB structure. The elastically strained tetragonal phase is labeled A. Signal originating from domain boundaries highlighted by the radial lines emanating from the central (044) RLP are labeled ρ, σ, τ and υ. The central figure is a 3D reconstruction of experimentally determined FWHMs of the corresponding peaks. (b) *H-K*, *H-L*, and *K-L* reciprocal space maps for the symmetric (004) reflection.

film can be found in Table I. The strain parameters in Table I are presented in terms of the Miller index mismatch. Note that the volume expansion for the orthorhombic phase (V/V_s=+0.013) is compensated by the volume decrease in the tetragonal phase (V/V_s=−0.022) thus minimizing the averaged volume change.

The full width at half maximum (FWHM) values in the *H-K* plane were determined and used to establish the in-plane correlation length of the CB film. Contributions due to coherent domain size on the peak breadth were decoupled from tilt-induced and twist-induced inhomogeneous variations of the unit cells. Both, the (022) and (044) reflections, which belong to the same family of crystallographic planes, were utilized in this analysis (see Ref. 11 for details). The in-plane correlation length $D_{H\text{-}K}$ for the CB domains has been estimated to be about $D_{H\text{-}K}\approx$25 nm, where $D_{H\text{-}K}$ $=a_S/\xi$, and ξ is the reflection-order-independent component of the peak's breadth. The *H-L* and *K-L* maps show that the CB peak breadths remain parallel to the sample surface and hence are dominated by size effects. Note that $D_{H\text{-}K}$ $\approx$25 nm is significantly larger than the typical size of the CB square of $\sim 4\times 4$ nm^2 [see transmission electron microscopy (TEM) in Ref. 5]. In the L direction, where inhomogeneous broadening due to composition fluctuations and film thickness in the growth direction should dominant the peak

TABLE I. Average lattice parameters and related *H-K-L* values of the different phases within the CB film are determined from multiple reflections. The lattice and volume mismatch for different phases is normalized to that for the reference spinel structure with a_s=0.8424 nm.

	$ZnMnGaO_4$ (Ref. 5) (bulk, $I41/amd$)	*A* (Transitional)	α/δ (Orthorhombic)	β,γ (Rotated tetr.)
$\Delta H/H$		0.00	−0.03/0.04	0.00
$\Delta K/K$		0.00	0.04/−0.03	0.00
$\Delta L/L$		0.023	0.016	0.016
a, nm	0.82	0.8424	0.898/0.814	0.841
b, nm	0.82	0.8424	0.814/0.898	0.841
c, nm	0.87	0.823	0.829	0.829
V/V_s	−0.022	−0.023	+0.013	−0.020
$FWHM_{H\text{-}K}$ (044)		0.01	0.13	0.13
$FWHM_L$ (044)		0.02	0.03	0.03
Rotation $\langle 00L\rangle$		0.00	0.00	±2.55°

breadth, the corresponding FWHM is significantly narrower $FWHM_L$=0.03 compared to the in-plane value. Compositional fluctuations are therefore believed to be relatively well controlled throughout the film. Contributions due to film thickness in the peak breadth can be considered negligible due to the thickness of the film in the growth direction.

The sharp peak labeled *A* at the center of the *H-K* map in Fig. 1(a) originates from a tetragonal phase that is lattice matched to the substrate. This transitional layer can be seen in Fig. 2, where the cross-sectional TEM image of the sample shows a homogeneous layer separating the MgO substrate and the CB film. The strain in this transitional layer is elastic as evident from the asymmetric (044) reflections. The corresponding *L* value for the *A* phase is equal to 4.095 ($\Delta L_A/L$=0.023; c_A=0.823 nm), which is greater than that of the α, β, γ, and δ phases (L=4.07, $\Delta L_{CB}/L$=0.016). Intensity of each α, β, γ, and δ peak for the (044) reflection has been integrated over their volumes in reciprocal space and are within 10% of each other. The total diffracted intensity for these four phases is approximately six times that for the narrow *A* peak. This ratio is consistent with the relative layer thickness as determined by TEM [Fig. 2], where the CB layer is 735 nm and the transitional layer *A* is only 85 nm thick. Comparison of the relative diffracted intensity and the lattice mismatch in the *L* direction supports the assignment of peak *A* as due to the thin transitional layer at the interface between the MgO substrate and the CB structure.

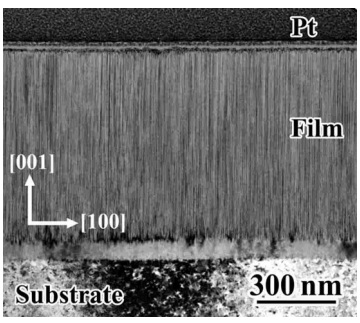

FIG. 2. Cross-sectional TEM image of the ZMGO film at low magnification. The homogenous transitional layer *A* can be seen directly above the MgO substrate followed by growth of the CB arranged ZMGO nanorods and a Pt capping layer for focusing of the ion beam. The vertical striations demonstrate the high alignment of the epitaxial growth of $4\times4\times735$ nm^3 nanorods.

Figures 3(a)–3(c) are *H-K* RSMs measured around the (−2−22), (022), and (−202) RLPs with L=2.04. The similarity between the (−202) and (022) reflections corresponds to a 90° rotational invariance (with translation) of the entire CB structure. All diffraction peaks for the (−2−22) reflection are closely aligned to the arc with a constant magnitude of the reciprocal-lattice vector with the radius of $R=2\sqrt{2}$ shown as a dashed line in Fig. 3(a). This observation corresponds to a close proximity of the *average* in-plane lattice parameter for all α, β, γ, and δ phases to that of the reference spinel structure; hence, the average in-plane parameter of the CB structure matches that of the MgO lattice. The orthorhombic and rotated tetragonal phases are separated by the domain boundaries (DB) closely aligned along the $\langle 110\rangle$ and $\langle 1-10\rangle$ directions as shown in Fig. 3(d). These domain walls should accommodate structural distortions between α, β, γ, and δ phases providing means for their coherence along both the film-growth direction and in-plane direction. From comparison of the in-plane domain size (4×4 nm^2) and the in-plane footprint of the spinel lattice ($\sim0.8\times0.8$ nm^2), the fraction of distorted unit cells at the DB to the number of undistorted cells inside each phase is significant: about 30%. Hence, these domain walls should also produce a significant contribution to the total diffraction picture. Thus, we assign the DB diffraction signal to four additional diagonal streaks labeled ρ, σ, τ, and υ positioned between the α, β, γ, and δ peaks in Figs. 1(a). The dashed lines in Fig. 3(d) define the CB supercell, which through translational operations can produce the entire CB film. The angles between the DB have been determined from angular separation between the ρ, σ, τ, and υ streaks in the *H-K* maps. The 90° angle between the υ-τ and ρ-σ streaks corresponds to domains with the twisted tetragonal phases, while the 97.5° and 82.5°

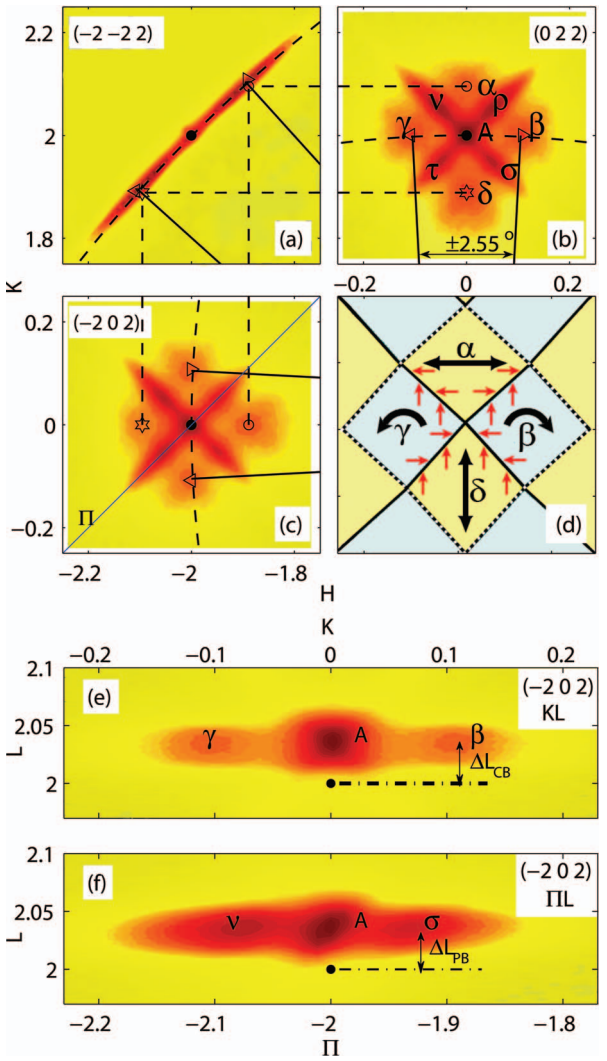

FIG. 3. (Color). (a), (b), and (c) *H*-*K* cross-sectional RSM measured around the (−2−22), (022), and (−202) RLPs; L=2.04. For illustrative purposes the (−2−22) map is converted to depict a (−222) reflection. The calculated positions for the α, β, γ, and δ phases in reciprocal space are labeled by open triangles, circles, and stars. The straight dashed lines illustrate projection of each phase within reciprocal space. The dashed arcs represent direction of rotation for the two tetragonal phases. (d) Illustration of the CB structure with atomic distortions within each domain represented by large black arrows. Atomic distortions at the DBs are shown by the smaller red (dark gray) arrows. The supercell of the CB structure is highlighted by the dashed contour. (e) The *K*-*L* and (f) Π-*L* cross-sectional map of the reciprocal space around the (−202) RLP, where Π is in the direction depicted by the diagonal line in Fig. 3(c).

separation of the ρ-τ and σ-υ streaks confirms presence of the twined (perpendicularly oriented) diamond-shaped domains containing the orthorhombic phases. Cross-sectional RSM were measured around the (−202) RLP in both the *K*-*L* and Π-*L* planes, Figs. 3(e) and 3(f), respectively, where $\Pi=(H+K)/\sqrt{2}$. These maps demonstrate that the out-plane lattice parameters for ρ, σ, τ, and υ are the same as that for the α, β, γ, and δ phases, as expected for coherent DB associated peaks.

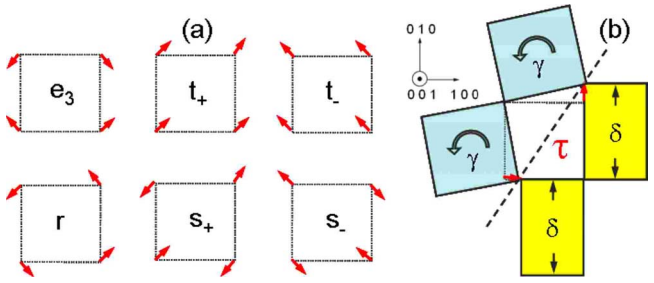

FIG. 4. (Color online). (a) The normal distortion modes of a monoatomic 2D square lattice. (b) Schematic of atomic distortions, red (dark gray) arrows, along ⟨100⟩ and ⟨010⟩ directions at domain boundary τ (dashed line). Squares γ and rectangles δ correspond to the rotated tetragonal and orthorhombic lattices, respectively.

IV. DISCUSSION

To better understand symmetry of the lattice distortions at the domain boundaries, it is useful to describe the *in-plane* CB pattern in terms of distortions with respect to a two-dimensional (2D) square lattice. The mode-based atomic-scale description of the lattice distortions has recently been developed for a 2D square lattice with a monatomic basis.[12,13] Six modes relevant to the CB pattern are shown in Fig. 4(a). Mode e_3 corresponds to square-to-rectangle distortions with a/b ratio $(1+e_3/\sqrt{2})/(1-e_3/\sqrt{2})$. If we represent $e_3=\varepsilon>0$ in the domain α, the domain δ, then has $e_3=-\varepsilon$. Mode r represents rotations by an angle of $r/\sqrt{2}$ radian. The amplitude for the rotation mode is $r=\varepsilon$ in the γ domain and $r=-\varepsilon$ for the β domain. The distortions at the DBs can be represented as a linear combination of e_3, r, and two other modes; either t_+ and s_+ or t_- and s_-. For example, distortions at the interface between the γ and δ domains, as illustrated in Fig. 4(b), can be characterized by a combination of the $-e_3+r+t_++s_+$ distortion modes with amplitudes of $e_3=-\varepsilon/2$, $r=\varepsilon/2$, $t_+=\varepsilon/2$, and $s_+=\varepsilon/2$. Among these four modes, e_3 and r are strain modes, repetition of which can fill the entire space and shift the corresponding diffraction peak around the undisturbed RLP. In contrast, s_+ is a short-wavelength (π,π) mode that should alternate its sign and double the unit cell to fill the entire space. Such short-wavelength distortions could result in redistribution of the x-ray intensity between different reflection orders and could generate superlattice peaks. Evidence of this can be seen by noting the stronger DB peaks from the (022) reflection in Figs. 3(b) and 3(c) compared to those for the (044) reflection in Fig. 1(a). Mode t_+ represents a rigid translation: the application of which does not change the x-ray diffraction pattern. Therefore, the distortions $e_3=-\varepsilon/2$ and $r=\varepsilon/2$ within the DB could shift the diffraction peak from the undisturbed RLP position to the point right between the peaks from domains δ and γ, which corresponds to peak τ in Figs. 1(a) and 3(b). If only scattering from a single domain interface is considered, the FWHM for DB peaks in the *H*-*K* plane should be very broad in the direction perpendicular to the boundary. The narrow breadth of the DB peaks, however, in the direction perpendicular to their major axis provides further experimental evidence of highly coherent growth among neighboring domains. Note that this observation is in agreement with the aforementioned large

value of the correlation length for all CB domains ($D_{H-K} \approx 25$ nm) that covers several identical DBs between the 4×4 nm^2 CB domains.

V. SUMMARY AND CONCLUDING REMARKS

In summary, the MgO substrate is covered by a thin elastically strained $ZnGaMnO_4$ layer with no phase separation (peak A), where the relaxation process begins as evident in the tail of peak A [Fig. 1(a)] between $\Delta L_A/L=0.023$ and $\Delta L_{CB}/L=0.017$. Eventually, accumulation of the volume strain energy results in partial relaxation of strain and formation of the elastically strained CB layer consisting of two conversely rotated tetragonal and two orthogonal orthorhombic phases (α, β, γ, and δ). The corners of the CB supercell match perfectly the MgO substrate, though influences from subgrain boundaries in the MgO substrate are not felt to be influential in the CB formation. The DBs, which are oriented along $\langle 110 \rangle$ and $\langle 1-10 \rangle$ directions, and separate orthorhombic and rotated tetragonal phases accommodate the structural disparities between the α, β, γ, and δ phases by means of lattice distortions shown in Fig. 4(b). The accommodating mechanism is produced by contributions from the Mn^{3+} ions, which become JT active upon occupying the octahedral sites in the spinel structure of the Mn-rich orthorhombic phase. The orbital degeneracy of the Mn ion ground state is lifted by structural distortions and the electric energy gain overcomes the cost of displacive structural energy.

Among open questions for the future theoretical analysis of the CB structures we mention modeling of the exact in-plane size of the pattern and the mechanisms of suppression of the herring-bone structure for films vs that in the bulk. Here we will only speculate that the size of the CB domains is determined by various competing factors. The energy cost associated with the formation DBs would favor bigger domains since the number of the strained lattice cells at the DBs relative to the number of undisturbed cells decreases inversely proportionally to the domain size. However, the domain size is limited from above by the diffusion length of Mn and Ga ions during the annealing, as indicated in a recent experiment on nano-CB formation of a Mn-doped $CoFe_2O_4$ spinel compound.[4] Other factors, such as the strain energy cost between the CB film and the substrate, would also influence the size of domains, giving rise to a nanometer length scale CB pattern and suppressing the herring-bone structure formation.

ACKNOWLEDGMENTS

Work at NJIT and Rutgers was supported by the DOE under Contract No. DE-FG02-07ER46382 and the NSF under Contract No. DMR-0546985. Work at the Cornell High Energy Synchrotron Source was supported by the NSF and the NIH/NIGMS under Grant No. DMR-0225180. The authors are thankful to Theo Siegrist for his interest and useful discussions.

*so26@njit.edu

[1] S. Yeo, Y. Horibe, S. Mori, C. M. Tseng, C. H. Chen, A. G. Khachaturyan, C. L. Zhang, and S.-W. Cheong, Appl. Phys. Lett. **89**, 233120 (2006).
[2] B. S. Guiton and P. K. Davies, Nature Mater. **6**, 586 (2007).
[3] C. L. Zhang, S. Yeo, Y. Horibe, Y. J. Choi, S. Guha, M. Croft, S.-W. Cheong, and S. Mori, Appl. Phys. Lett. **90**, 133123 (2007).
[4] C. L. Zhang, C. M. Tseng, C. H. Chen, S. Yeo, Y. J. Choi, and S.-W. Cheong, Appl. Phys. Lett. **91**, 233110 (2007).
[5] S. Park, Y. Horibe, T. Asada, L. S. Wielunski, N. Lee, P. L. Bonanno, S. M. O'Malley, A. A. Sirenko, A. Kazimirov, M. Tanimura, T. Gustafsson, and S.-W. Cheong, Nano Lett. **8**, 720 (2008).
[6] J. L. MacManus-Driscoll, P. Zerrer, H. Wang, H. Yang, J. Yoon, A. Fouchet, R. Yu, M. G. Blamire, and Q. X. Jia, Nature Mater. **7**, 314 (2008).
[7] H. Zheng, Q. Zhan, F. Zavaliche, M. Sherburne, F. Straub, M. P. Cruz, L.-Q. Chen, U. Dahmen, and R. Ramesh, Nano Lett. **6**, 1401 (2006).
[8] Y. Ni, Y. M. Jin, and A. G. Khachaturyan, Acta Mater. **55**, 4903 (2007).
[9] M. A. Ivanov, N. K. Tkachev, and A. Ya. Fishman, Low Temp. Phys. **25**, 459 (1999).
[10] For a discrete tilt of the tetragonal phases from the [001] direction, the β and γ peaks should have appeared in both the (044) and (004) RSMs.
[11] E. J. Mittemeijer and P. Scardi, *Diffraction Analysis of the Microstructure of Materials* (Springer, New York, 2004).
[12] K. H. Ahn, T. Lookman, A. Saxena, and A. R. Bishop, Phys. Rev. B **68**, 092101 (2003).
[13] J. Moon, T. F. Seman, and K. H. Ahn, arXiv:0707.1921 (unpublished).